

# Merging Compact Binaries Near a Rotating Supermassive Black Hole: Eccentricity Excitation due to Apsidal Precession Resonance

Bin Liu<sup>1</sup>, Dong Lai<sup>1</sup>

<sup>1</sup> *Cornell Center for Astrophysics and Planetary Science, Cornell University, Ithaca, NY 14853, USA*

We study the dynamics of merging compact binaries near a rotating supermassive black hole (SMBH) in a hierarchical triple configuration. We include various general relativistic effects that couple the inner orbit, the outer orbit and the spin of the SMBH. During the orbital decay due to gravitational radiation, the inner binary can encounter an “apsidal precession resonance” and experience eccentricity excitation. This resonance occurs when the apsidal precession rate of the inner binary matches that of the outer binary, with the precessions driven by both Newtonian interactions and various post-Newtonian effects. The eccentricity excitation requires the outer orbit to have a finite eccentricity, and is most effective for triples with small mutual inclinations, in contrast to the well-studied Lidov-Kozai effect. The resonance and the associated eccentricity growth may occur while the binary emits gravitational waves in the low-frequency band, and may be detectable by future space-based gravitational wave detectors.

## I. INTRODUCTION

The detections of gravitational waves from merging binary black holes (BHs) [1–5] have motivated many recent studies on their formation channels. These include the traditional isolated binary evolution [e.g., 6–13] and chemically homogeneous evolution [e.g., 14, 15], gas-assisted mergers [e.g., 16], and various flavors of dynamical channels that involve either strong gravitational scatterings in dense clusters [e.g., 17–27] or more gentle “tertiary-induced mergers” [e.g., 28–38]. Many recent studies have shown that merging BH and neutron star (NS) binaries can be formed efficiently (via Lidov-Kozai (LK) oscillations [39–41]) with the aid of a tertiary body that moves on an inclined (outer) orbit relative to the orbit of the inner binary. Furthermore, the efficiency of the merger can be enhanced when the triple is part of a quadruple system [e.g., 42–45], or more generally, when the outer orbit experiences quasi-periodic external forcing [e.g., 46–48].

In the standard LK-induced merger scenario, the leading order of post-Newtonian (PN) effect of general relativity (GR) gives rise to apsidal precession of the inner binary, and this tends to suppress LK oscillations or limit the maximum eccentricity [e.g., 49–51]. However, several numerical studies [e.g., 52–54] based on secular triple equations (see [55–57] for recent, more systematic study of the secular triple equations in PN theory) also found evidence that with small mutual inclinations (no LK oscillations are allowed to occur), significant eccentricity excitation might still be achieved under some conditions (e.g., the clearest example of this phenomenon is displayed in Figure 14 of [52]; [54] added some other (generally non-essential) PN terms and called this “GR-induced eccentricity excitation”). The physical explanation of the eccentricity growth at low inclinations in terms of “apsidal precession resonance” was provided in [58] in the context of merging compact binaries with tertiary (low-mass) companions. It was shown that a secular resonance occurs when the total apsidal precession

of the inner binary (driven by GR and the outer binary) matches the precession rate of the outer binary (driven by the inner binary), and this resonance allows efficient “transfer” of eccentricity from the outer binary to the inner binary.

In this paper, we are interested in stellar-mass BH binary (BHB) mergers induced by a supermassive BH (SMBH). Such BHBs may exist in abundance in the nuclear cluster (with a central SMBH) due to various dynamical processes, i.e., scatterings and mass segregation [59, 60]. Importantly, our recent study [61] shows that several GR effects (including some of the “cross terms” studied in [55]) introduced by a rotating SMBH can generate extra precessions on the BH orbits, significantly increasing the merger fraction (as well as the merger rate). This opens the question of how these GR effects modify the eccentricity growth mechanism due to the “apsidal precession resonance”. We address this issue systematically in this paper. We focus our attention to isolated BHB-SMBH triple systems, and do not consider other processes related to scatterings and relaxation with surrounding stars in the cluster [47, 62, 63], which may also change the character of SMBH-induced mergers of stellar BHBs.

Our paper is organized as follows. In Section II, we review the essential GR effects (including the “cross terms”) relevant to BHB-SMBH triples and present the secular equations in PN theory. In Section III, we present some numerical examples to illustrate how secular apsidal resonance influences the orbital decay of BHB in triples. In Section IV, we perform analytical calculations for the eccentricity excitation for coplanar systems residing near the resonance, and explore the parameter space which can lead to the eccentricity excitation. In Section V, we extend our calculations to systems with slightly inclined outer binary and spin orientations. We summarize our main results in Section VI.

## II. EVOLUTION OF BHB NEAR A SMBH

### A. Equations for Standard LK-Induced Merger

We consider a hierarchical triple system, composed of an inner BH binary of masses  $m_1$ ,  $m_2$  and a distant companion (the SMBH) of mass  $m_3$  that moves around the center of mass of the inner bodies. The reduced mass for the inner binary is  $\mu_{\text{in}} \equiv m_1 m_2 / m_{12}$ , with  $m_{12} \equiv m_1 + m_2$ . Similarly, the outer binary has  $\mu_{\text{out}} \equiv (m_{12} m_3) / m_{123}$  with  $m_{123} \equiv m_{12} + m_3$ . The semi-major axes and eccentricities are denoted by  $a_{\text{in}}$ ,  $a_{\text{out}}$  and  $e_{\text{in}}$ ,  $e_{\text{out}}$ , respectively. Therefore, the orbital angular momenta of two orbits are given by  $\mathbf{L}_{\text{in}} = L_{\text{in}} \hat{\mathbf{L}}_{\text{in}} = \mu_{\text{in}} \sqrt{G m_{12} a_{\text{in}} (1 - e_{\text{in}}^2)} \hat{\mathbf{L}}_{\text{in}}$  and  $\mathbf{L}_{\text{out}} = L_{\text{out}} \hat{\mathbf{L}}_{\text{out}} = \mu_{\text{out}} \sqrt{G m_{123} a_{\text{out}} (1 - e_{\text{out}}^2)} \hat{\mathbf{L}}_{\text{out}}$ . We define the mutual inclination between  $\mathbf{L}_{\text{in}}$  and  $\mathbf{L}_{\text{out}}$  (inner and outer orbits) as  $I$ . Throughout the paper, for convenience of notation, we will frequently omit the subscript ‘‘in’’ for the inner orbit.

To study the evolution of the merging inner BH binary under the influence of the tertiary companion, we use the double-averaged (DA; averaging over both the inner and outer orbital periods) secular equations of motion. For the nearly coplanar systems studied in his paper, the inner binary never reaches eccentricity close to unity, the DA approximation is valid (see section 2.1 of [38]). For the inner binary, the dynamics of the angular momentum  $\mathbf{L}$  and eccentricity  $\mathbf{e}$  vectors are given by

$$\frac{d\mathbf{L}}{dt} = \frac{d\mathbf{L}}{dt} \Big|_{\text{LK}} + \frac{d\mathbf{L}}{dt} \Big|_{\text{GW}}, \quad (1)$$

$$\frac{d\mathbf{e}}{dt} = \frac{d\mathbf{e}}{dt} \Big|_{\text{LK}} + \frac{d\mathbf{e}}{dt} \Big|_{\text{GR}} + \frac{d\mathbf{e}}{dt} \Big|_{\text{GW}}, \quad (2)$$

where we include the contributions from the Newtonian potential of the external companion (the first terms in Equations (1)-(2)); following the notation of [38], we label these with the subscript ‘‘LK’’ since they can generate LK oscillations for sufficiently inclined orbits – although in this paper we focus on non-LK regime), the leading order PN correction, and the dissipation due to gravitational waves (GW) emission.

The explicit DA equations of  $d\mathbf{L}/dt|_{\text{LK}}$  and  $d\mathbf{e}/dt|_{\text{LK}}$ , are provided in [50]. The Newtonian (LK) terms induce precession of eccentricity vectors on the timescale

$$T_{\text{LK}} = \frac{1}{\omega_{\text{LK}}} = \frac{1}{n} \frac{m_{12}}{m_3} \left( \frac{a_{\text{out,eff}}}{a} \right)^3, \quad (3)$$

where  $n = (Gm_{12}/a^3)^{1/2}$  is the mean motion of the inner binary, and  $a_{\text{out,eff}} \equiv a_{\text{out}} \sqrt{1 - e_{\text{out}}^2}$  is the effective outer binary separation. Again, we label this  $T_{\text{LK}}$ , because for sufficiently inclined orbits, this is the LK timescale for oscillations in eccentricity and orbital inclination.

GR (1-PN correction) introduces pericenter precession

of the inner binary,

$$\frac{d\mathbf{e}}{dt} \Big|_{\text{GR}} = \omega_{\text{GR,in}} \hat{\mathbf{L}} \times \mathbf{e}, \quad (4)$$

with the precession rate

$$\omega_{\text{GR,in}} = \frac{3G^{3/2} m_{12}^{3/2}}{c^2 a^{5/2} (1 - e^2)}. \quad (5)$$

Similar equations apply to the outer binary, with

$$\frac{d\mathbf{e}_{\text{out}}}{dt} \Big|_{\text{GR}} = \omega_{\text{GR,out}} \hat{\mathbf{L}}_{\text{out}} \times \mathbf{e}_{\text{out}}, \quad (6)$$

$$\omega_{\text{GR,out}} = \frac{3G^{3/2} m_{123}^{3/2}}{c^2 a_{\text{out}}^{5/2} (1 - e_{\text{out}}^2)}. \quad (7)$$

During the LK oscillations, the short-range effect captured in Equation (4) plays a crucial role in determining the maximum eccentricity  $e_{\text{max}}$  of the inner binary [e.g., 49], that can be evaluated analytically [e.g., 50, 51].

Gravitational radiation draws energy and angular momentum from the BH orbit. The rates of change of  $\mathbf{L}$  and  $\mathbf{e}$  are given by [64]

$$\frac{d\mathbf{L}}{dt} \Big|_{\text{GW}} = -\frac{32}{5} \frac{G^{7/2}}{c^5} \frac{\mu^2 m_{12}^{5/2}}{a^{7/2}} \frac{1 + 7e^2/8}{(1 - e^2)^2} \hat{\mathbf{L}}, \quad (8)$$

$$\frac{d\mathbf{e}}{dt} \Big|_{\text{GW}} = -\frac{304}{15} \frac{G^3}{c^5} \frac{\mu m_{12}^2}{a^4 (1 - e^2)^{5/2}} \left( 1 + \frac{121}{304} e^2 \right) \mathbf{e}. \quad (9)$$

For reference, the merger time due to GW radiation of an isolated binary with the initial semi-major axis  $a_0$  and eccentricity  $e_0$  is approximately given by

$$\begin{aligned} T_{\text{m}} &= T_{\text{m},0} (1 - e_0^2)^{7/2} = \frac{5c^5 a_0^4}{256 G^3 m_{12}^2 \mu} (1 - e_0^2)^{7/2} \quad (10) \\ &\simeq 10^{10} \left( \frac{60 M_{\odot}}{m_{12}} \right)^2 \left( \frac{15 M_{\odot}}{\mu} \right) \left( \frac{a_0}{0.2 \text{AU}} \right)^4 (1 - e_0^2)^{7/2} \text{yrs.} \end{aligned}$$

Equations (1)-(2), as well as the similar equations of motion of the outer binary (without GW emission), completely determine the evolution of the triple system. The *Standard LK-Induced Merger* mechanism (as studied in most previous works) considers sufficiently large mutual inclinations, and includes the apsidal precession due to GR (Equation (4)), but neglects the GR effects associated with the rotating tertiary companion. This is adequate when the tertiary mass  $m_3$  is not much larger than the masses of the inner BHB. However, for BHB-SMBH triples, with  $m_3 \gg m_1, m_2$ , several GR effects involving the SMBH can qualitatively change the efficiency and outcomes of LK-induced mergers [61].

### B. Additional GR effects due to rotating SMBH

For a rotating SMBH, the spin angular momentum is given by  $S_3 = \chi_3 G m_3^2 / c$ , where  $\chi_3 \leq 1$  is the Kerr parameter (we set  $\chi_3 = 1$  in the numerical examples presented this paper). In GR, the vectors  $\mathbf{L}$ ,  $\mathbf{L}_{\text{out}}$ ,  $\mathbf{S}_3$ ,  $\mathbf{e}$

and  $\mathbf{e}_{\text{out}}$  are coupled to each other, inducing time evolution of these vectors. In a systematical post-Newtonian framework of triple dynamics [55–57], there are numerous terms. We summarize the most essential effects below (also the leading-order effects). The related equations are either from the classical work on binaries with spinning bodies [65] (see also [66] and references therein), or can be derived (or extended to include eccentricity) “by analogy”, i.e., by recognizing that the inner binary’s orbital angular momentum  $\mathbf{L}$  behaves like a “spin”. As we see below, the vector forms of the equations we use are much more transparent than equations based on orbital elements (see [55–57]), especially we are deal with misaligned  $\mathbf{L}$ ,  $\mathbf{L}_{\text{out}}$  and  $\mathbf{S}_3$ .

*Effect I: the coupling between  $\mathbf{L}_{\text{out}}$  and  $\mathbf{S}_3$ .* In the BHB-SMBH system, the angular momentum of the outer binary  $\mathbf{L}_{\text{out}}$  and the spin angular momentum  $\mathbf{S}_3$  of  $m_3$  precesses around each other due to spin-orbit coupling if the two vectors are misaligned (1.5 PN effect) [65, 67]:

$$\left. \frac{d\mathbf{L}_{\text{out}}}{dt} \right|_{\mathbf{L}_{\text{out}}\mathbf{S}_3} = \omega_{\mathbf{L}_{\text{out}}\mathbf{S}_3} \hat{\mathbf{S}}_3 \times \mathbf{L}_{\text{out}}, \quad (11)$$

$$\left. \frac{d\mathbf{e}_{\text{out}}}{dt} \right|_{\mathbf{L}_{\text{out}}\mathbf{S}_3} = \omega_{\mathbf{L}_{\text{out}}\mathbf{S}_3} \hat{\mathbf{S}}_3 \times \mathbf{e}_{\text{out}} - 3\omega_{\mathbf{L}_{\text{out}}\mathbf{S}_3} (\hat{\mathbf{L}}_{\text{out}} \cdot \hat{\mathbf{S}}_3) \hat{\mathbf{L}}_{\text{out}} \times \mathbf{e}_{\text{out}} \quad (12)$$

$$\left. \frac{d\hat{\mathbf{S}}_3}{dt} \right|_{\mathbf{S}_3\mathbf{L}_{\text{out}}} = \omega_{\mathbf{S}_3\mathbf{L}_{\text{out}}} \hat{\mathbf{L}}_{\text{out}} \times \hat{\mathbf{S}}_3, \quad (13)$$

where the orbit-averaged precession rates are

$$\omega_{\mathbf{L}_{\text{out}}\mathbf{S}_3} = \frac{GS_3(4 + 3m_{12}/m_3)}{2c^2a_{\text{out}}^3(1 - e_{\text{out}}^2)^{3/2}} = \omega_{\mathbf{S}_3\mathbf{L}_{\text{out}}} \frac{S_3}{L_{\text{out}}}. \quad (14)$$

Since in our case,  $S_3$  can be easily larger than  $L_{\text{out}}$ , the de-Sitter precession (Equation (13)) is negligible.

*Effect II: the coupling between  $\mathbf{L}$  and  $\mathbf{L}_{\text{out}}$ .* In addition to the Newtonian precession (driven by the tidal potential of  $m_3$ ),  $\mathbf{L}$  experiences an additional de-Sitter like (geodesic) precession in the gravitational field of  $m_3$  introduced by GR. This is a 1.5 PN spin-orbit coupling effect, with  $\mathbf{L}$  behaving like a “spin”. We have

$$\left. \frac{d\mathbf{L}}{dt} \right|_{\mathbf{L}_{\text{in}}\mathbf{L}_{\text{out}}} = \omega_{\mathbf{L}_{\text{in}}\mathbf{L}_{\text{out}}}^{(\text{GR})} \hat{\mathbf{L}}_{\text{out}} \times \mathbf{L}, \quad (15)$$

$$\left. \frac{d\mathbf{e}}{dt} \right|_{\mathbf{L}_{\text{in}}\mathbf{L}_{\text{out}}} = \omega_{\mathbf{L}_{\text{in}}\mathbf{L}_{\text{out}}}^{(\text{GR})} \hat{\mathbf{L}}_{\text{out}} \times \mathbf{e}, \quad (16)$$

and the feedback from  $\hat{\mathbf{L}}$ ,  $\mathbf{e}$  on  $\mathbf{L}_{\text{out}}$  and  $\mathbf{e}_{\text{out}}$  are given by (see [65])

$$\left. \frac{d\mathbf{L}_{\text{out}}}{dt} \right|_{\mathbf{L}_{\text{out}}\mathbf{L}_{\text{in}}} = \omega_{\mathbf{L}_{\text{out}}\mathbf{L}_{\text{in}}}^{(\text{GR})} \hat{\mathbf{L}} \times \mathbf{L}_{\text{out}}, \quad (17)$$

$$\left. \frac{d\mathbf{e}_{\text{out}}}{dt} \right|_{\mathbf{L}_{\text{out}}\mathbf{L}_{\text{in}}} = \omega_{\mathbf{L}_{\text{out}}\mathbf{L}_{\text{in}}}^{(\text{GR})} \hat{\mathbf{L}} \times \mathbf{e}_{\text{out}} - 3\omega_{\mathbf{L}_{\text{out}}\mathbf{L}_{\text{in}}}^{(\text{GR})} (\hat{\mathbf{L}}_{\text{out}} \cdot \hat{\mathbf{L}}) \hat{\mathbf{L}}_{\text{out}} \times \mathbf{e}_{\text{out}}, \quad (18)$$

with

$$\omega_{\mathbf{L}_{\text{in}}\mathbf{L}_{\text{out}}}^{(\text{GR})} = \frac{3G(m_3 + \mu_{\text{out}}/3)n_{\text{out}}}{2c^2a_{\text{out}}(1 - e_{\text{out}}^2)} = \omega_{\mathbf{L}_{\text{out}}\mathbf{L}_{\text{in}}}^{(\text{GR})} \frac{L_{\text{out}}}{L}, \quad (19)$$

where  $n_{\text{out}} = (Gm_{\text{tot}}/a_{\text{out}}^3)^{1/2}$ . Note the similarity between Equations (17)-(18) and Equations (11)-(12).

Note that both Equations (15)-(16) are required to keep  $\mathbf{L} \cdot \mathbf{e} = 0$ . Equations (15)-(16) can also be reproduced through the “cross terms” in the PN equations of motion of hierarchical triple systems [55, 56].

*Effects III: the coupling between  $\mathbf{L}$  and  $\mathbf{S}_3$ .* Since the semimajor axis of the inner orbit ( $a$ ) is much smaller than the outer orbit ( $a_{\text{out}}$ ), the inner binary can be treated as a single body approximately. Therefore, the angular momentum  $\hat{\mathbf{L}}$  is coupled to the spin angular momentum  $\mathbf{S}_3$  of  $m_3$ , and experiences Lens-Thirring precession. This is a 2 PN spin-spin coupling effect, with  $\mathbf{L}$  behaving like a “spin”. We have

$$\left. \frac{d\mathbf{L}}{dt} \right|_{\mathbf{L}_{\text{in}}\mathbf{S}_3} = \omega_{\mathbf{L}_{\text{in}}\mathbf{S}_3} \hat{\mathbf{S}}_3 \times \mathbf{L} - 3\omega_{\mathbf{L}_{\text{in}}\mathbf{S}_3} (\hat{\mathbf{L}}_{\text{out}} \cdot \hat{\mathbf{S}}_3) \hat{\mathbf{L}}_{\text{out}} \times \mathbf{L}, \quad (20)$$

$$\left. \frac{d\mathbf{e}}{dt} \right|_{\mathbf{L}_{\text{in}}\mathbf{S}_3} = \omega_{\mathbf{L}_{\text{in}}\mathbf{S}_3} \hat{\mathbf{S}}_3 \times \mathbf{e} - 3\omega_{\mathbf{L}_{\text{in}}\mathbf{S}_3} (\hat{\mathbf{L}}_{\text{out}} \cdot \hat{\mathbf{S}}_3) \hat{\mathbf{L}}_{\text{out}} \times \mathbf{e}. \quad (21)$$

Note that Equation (21) is required to keep  $\mathbf{L} \cdot \mathbf{e} = 0$ . The back-reaction on the outer binary is gives (see Equations 64,65,70 of [65])

$$\left. \frac{d\mathbf{L}_{\text{out}}}{dt} \right|_{\mathbf{S}_3\mathbf{L}_{\text{in}}} = -3\omega_{\mathbf{S}_3\mathbf{L}_{\text{in}}} \left[ (\hat{\mathbf{L}}_{\text{out}} \cdot \hat{\mathbf{L}}) \hat{\mathbf{S}}_3 + (\hat{\mathbf{L}}_{\text{out}} \cdot \hat{\mathbf{S}}_3) \hat{\mathbf{L}} \right] \times \mathbf{L}_{\text{out}}, \quad (22)$$

$$\left. \frac{d\mathbf{e}_{\text{out}}}{dt} \right|_{\mathbf{S}_3\mathbf{L}_{\text{in}}} = -3\omega_{\mathbf{S}_3\mathbf{L}_{\text{in}}} \left\{ (\hat{\mathbf{L}}_{\text{out}} \cdot \hat{\mathbf{L}}) \hat{\mathbf{S}}_3 + (\hat{\mathbf{L}}_{\text{out}} \cdot \hat{\mathbf{S}}_3) \hat{\mathbf{L}} + \left[ (\hat{\mathbf{L}} \cdot \hat{\mathbf{S}}_3) - 5(\hat{\mathbf{L}}_{\text{out}} \cdot \hat{\mathbf{L}})(\hat{\mathbf{L}}_{\text{out}} \cdot \hat{\mathbf{S}}_3) \right] \hat{\mathbf{L}}_{\text{out}} \right\} \times \mathbf{e}_{\text{out}}. \quad (23)$$

In the above, the orbit-averaged precession rates are

$$\omega_{\mathbf{L}_{\text{in}}\mathbf{S}_3} = \frac{GS_3}{2c^2a_{\text{out}}^3(1 - e_{\text{out}}^2)^{3/2}} = \omega_{\mathbf{S}_3\mathbf{L}_{\text{in}}} \frac{L_{\text{out}}}{L}. \quad (24)$$

Note  $\omega_{\mathbf{L}_{\text{in}}\mathbf{S}_3}/\omega_{\mathbf{L}_{\text{in}}\mathbf{L}_{\text{out}}}^{(\text{GR})} \sim (V_{\text{out}}/c)\chi_3$  (where  $V_{\text{out}}$  is the orbital velocity of the outer binary and  $\chi_3$  is the dimensionless spin parameter of the SMBH). Thus Effect III is important only when the outer binary is relativistic.

### III. MERGING BHB WITH A COPLANAR SMBH: NUMERICAL EXAMPLES

We begin with coplanar systems ( $\hat{\mathbf{L}} = \hat{\mathbf{L}}_{\text{out}}$ ) with the SMBH spin either aligned ( $\hat{\mathbf{S}}_3 = \hat{\mathbf{L}}$ ) or anti-aligned

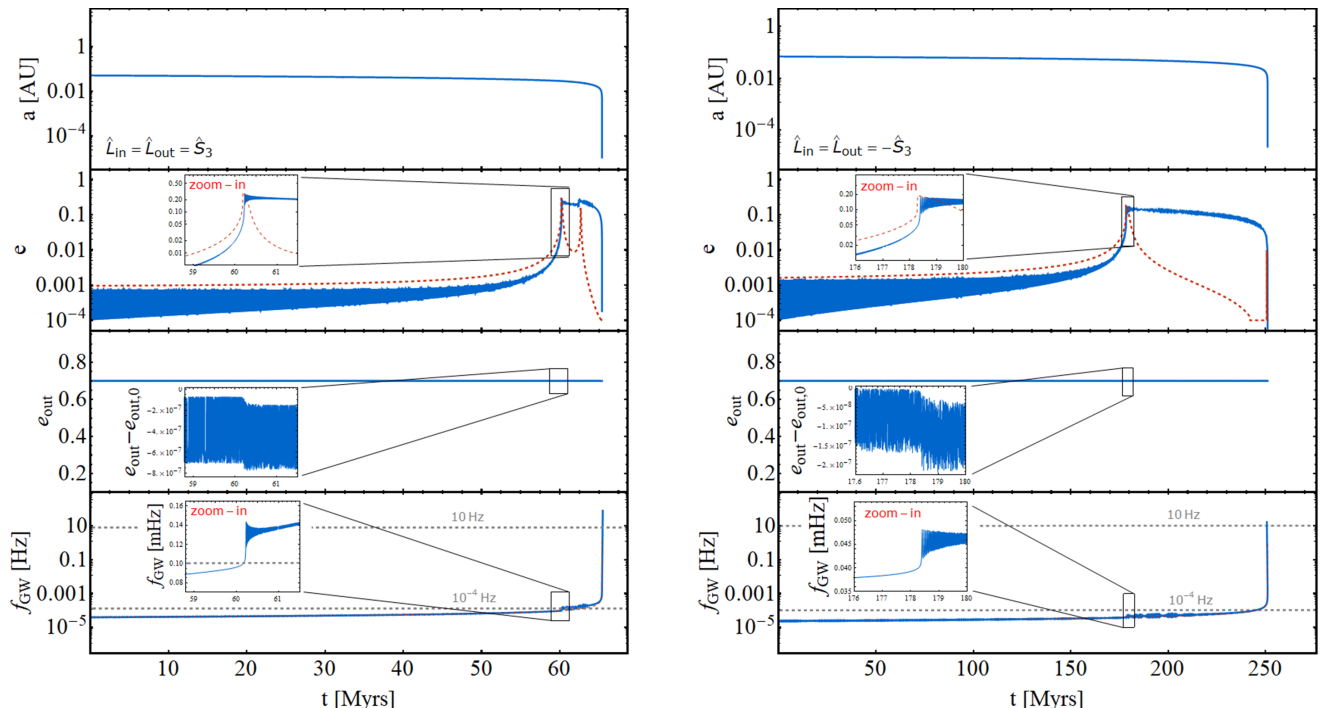


FIG. 1: The evolution of an inner merging BH-BH binary near a rotating SMBH in a coplanar orbital configuration, with the SMBH spin either parallel (left) or anti-parallel (right) to the orbits. The masses of BHs are  $m_1 = 30M_\odot$ ,  $m_2 = 20M_\odot$ , and  $m_3 = 10^6 M_\odot$ , respectively. The initial semimajor axes of the inner and outer binaries are  $a_0 = 0.05\text{AU}$  (left panel),  $a_0 = 0.07\text{AU}$  (right panel) and  $a_{\text{out}} = 90\text{AU}$ , respectively. The eccentricities and longitudes of the periapsis of two orbits are initialized as  $e_0 = 10^{-4}$ ,  $e_{\text{out},0} = 0.7$  and  $\varpi_0 = \varpi_{\text{out},0} = 0$ , respectively. The blue lines are obtained by the numerical integrations of the time evolution equations. The red-dashed lines on the second panels depict the analytical maximum eccentricity of the inner binary at the corresponding semi-major axis (see Section IV B). The subfigures in the third and bottom panels show the difference of outer eccentricity ( $e_{\text{out}} - e_{\text{out},0}$ ) and zoom-in of the GW peak frequency near the apsidal precession resonance.

( $\hat{\mathbf{S}}_3 = -\hat{\mathbf{L}}$ ) with respect to the orbit. Figure 1 shows two examples. All Newtonian (up to the octupole order) and GR effects discussed in Section II are included in the calculation. In the left panels (with  $\hat{\mathbf{L}} = \hat{\mathbf{L}}_{\text{out}} = \hat{\mathbf{S}}_3$ ), the eccentricity of the inner binary is negligible initially, but undergoes small-amplitude oscillations at the early phase, due to the Newtonian perturbation from the outer binary. During the orbital decay, the eccentricity gets excited twice and achieves a value of  $\sim 0.27$ . This is the result of the “apsidal precession resonance”, which allows the inner binary to efficiently “gain” some eccentricity from the outer binary (the eccentricity of the outer binary is initially 0.7, and decreases only slightly as the system passes through the resonance) (see more details in Section IV C). The bottom panel shows the time evolution of the peak frequency of GW, given by [30]

$$f_{\text{GW}} = \frac{(1+e)^{1.1954}}{\pi} \sqrt{\frac{G(m_{12})}{a^3(1-e^2)^3}}. \quad (25)$$

We see that the peak frequency is above  $10^{-4}$  Hz at resonance, and thus the system might be detected by the future gravitational wave detectors operating at low frequencies. After the resonances, the gravitational radiation reduces  $e$  gradually, circularizing the inner binary

before the final merger.

For reference, the right panel of Figure 1 shows the evolution for a system with  $\hat{\mathbf{L}} = \hat{\mathbf{L}}_{\text{out}} = -\hat{\mathbf{S}}_3$ . A similar resonance feature occurs, although at different location (semi-major axis), and the inner binary eccentricity builds up to as high as 0.18.

#### IV. APSIDAL PRECESSION RESONANCE: ANALYTICAL RESULTS FOR COPLANAR SYSTEMS

For coplanar ( $\hat{\mathbf{L}} = \hat{\mathbf{L}}_{\text{out}}$ ), non-dissipative (with no gravitational radiation) systems, the secular dynamics can be understood analytically. We first consider the case of small eccentricities, before studying the finite eccentricity case.

##### A. Linear (low- $e$ ) Systems

For systems with  $e, e_{\text{out}} \ll 1$ , the evolution of  $\mathbf{e}$  and  $\mathbf{e}_{\text{out}}$  is governed by the linear Laplace-Lagrange equations [68], with proper inclusion of the related GR precession

terms [58]. Define the complex eccentricity variables

$$\mathcal{E}_{\text{in}} = e_{\text{in}} \exp(i\varpi_{\text{in}}), \quad \mathcal{E}_{\text{out}} = e_{\text{out}} \exp(i\varpi_{\text{out}}), \quad (26)$$

where  $\varpi_{\text{in}}$ ,  $\varpi_{\text{out}}$  are the longitude of pericenter of the inner and outer orbits. The evolution equations are

$$\frac{d}{dt} \begin{pmatrix} \mathcal{E}_{\text{in}} \\ \mathcal{E}_{\text{out}} \end{pmatrix} = i \begin{pmatrix} \omega_{\text{in}} & \nu_{\text{in,out}} \\ \nu_{\text{out,in}} & \omega_{\text{out}} \end{pmatrix} \begin{pmatrix} \mathcal{E}_{\text{in}} \\ \mathcal{E}_{\text{out}} \end{pmatrix}, \quad (27)$$

where

$$\omega_{\text{in}} = \frac{3}{4} n \frac{m_3}{m_{12}} \left( \frac{a}{a_{\text{out}}} \right)^3 + \omega_{\text{GR,in}} + \omega_{\text{L}_{\text{in}}\text{L}_{\text{out}}}^{(\text{GR})} \mp 2\omega_{\text{L}_{\text{in}}\text{S}_3}, \quad (28)$$

$$\omega_{\text{out}} = \frac{3}{4} n_{\text{out}} \frac{m_1 m_2}{m_{12}^2} \left( \frac{a}{a_{\text{out}}} \right)^2 + \omega_{\text{GR,out}} \mp 2\omega_{\text{L}_{\text{out}}\text{S}_3} - 2\omega_{\text{L}_{\text{out}}\text{L}_{\text{in}}}^{(\text{GR})} \pm 6\omega_{\text{S}_3\text{L}_{\text{in}}}, \quad (29)$$

$$\nu_{\text{in,out}} = -\frac{15}{16} n \left( \frac{a}{a_{\text{out}}} \right)^4 \frac{m_3(m_1 - m_2)}{m_{12}^2}, \quad (30)$$

$$\nu_{\text{out,in}} = -\frac{15}{16} n_{\text{out}} \left( \frac{a}{a_{\text{out}}} \right)^3 \frac{m_1 m_2 (m_1 - m_2)}{m_{12}^3}. \quad (31)$$

where in Equations (28)-(29) the upper sign denotes the case of  $\hat{\mathbf{L}} = \hat{\mathbf{L}}_{\text{out}} = \hat{\mathbf{S}}_3$ , and the lower sign the  $\hat{\mathbf{L}} = \hat{\mathbf{L}}_{\text{out}} = -\hat{\mathbf{S}}_3$  case.

Starting with  $e_0 = 0$ ,  $e_{\text{out}} = e_{\text{out},0}$  at  $t = 0$ , Equation (27) can be solved to determine the time evolution of  $e(t)$  [see 58]. We find that  $e(t)$  oscillates between  $e_0$  and  $e_{\text{max}}$ , given by

$$e_{\text{max}} = 2e_{\text{out},0} \frac{|\nu_{\text{in,out}}|}{\sqrt{(\omega_{\text{in}} - \omega_{\text{out}})^2 + 4\nu_{\text{in,out}}\nu_{\text{out,in}}}}. \quad (32)$$

Clearly,  $e_{\text{max}}$  attains the peak value when  $\omega_{\text{in}} = \omega_{\text{out}}$ , at which

$$\begin{aligned} e_{\text{peak}} &= e_{\text{out},0} \left| \frac{\nu_{\text{in,out}}}{\nu_{\text{out,in}}} \right|^{1/2} = e_{\text{out},0} \left| \frac{L'_{\text{out}}}{L'_{\text{in}}} \right|^{1/2} \\ &= e_{\text{out},0} \frac{m_{12}^{3/4}}{m_{123}^{1/4}} \frac{m_3^{1/2}}{(m_1 m_2)^{1/2}} \left( \frac{a_{\text{out}}}{a} \right)^{1/4}, \quad (33) \end{aligned}$$

where  $L'_{\text{in}} = L_{\text{in}}(e = 0)$  and  $L'_{\text{out}} = L_{\text{out}}(e_{\text{out}} = 0)$ . We call this ‘‘apsidal precession resonance’’.

The linear theory is valid only for  $e \ll 1$  and  $e_{\text{out}} \ll 1$ . Equation (33) shows that when  $L'_{\text{out}} \gg L'_{\text{in}}$ , as in the cases studied in this paper ( $m_3 \gg m_1, m_2$ ), even a small  $e_{\text{out},0}$  may lead to unphysically larger  $e_{\text{peak}}$ . In practice, Equation (33) is useful in the sense that whenever it predicts  $e_{\text{peak}}$  of order unity or larger, we can expect the inner binary to attain significant eccentricity, but the precise value of  $e$  can only be obtained using nonlinear calculations, as we discuss next.

## B. Finite Eccentricities

For finite eccentricities, Equation (27) breaks down, but the eccentricity evolution of a coplanar triple can still be understood using energy and angular momentum conservations, without the need of numerical integrations of the equations of motion.

The total energy of the triple can be written as  $\Phi_{\text{tot}} = \Phi_{\text{N}} + \Phi_{\text{extra}}$ , where

$$\Phi_{\text{N}} = \frac{\mu\Phi_0}{8} \left[ -2 - 3e^2 - \frac{15}{8} \varepsilon_{\text{oct}} e(4 + 3e^2) \cos \Delta\varpi \right] \quad (34)$$

is the Newtonian potential energy between the inner and outer orbits in the octupole order [52, 58, 69], and  $\Phi_{\text{extra}}$  is the effective energy associated to the GR effects. In Equation (34),  $\Delta\varpi \equiv \varpi_{\text{in}} - \varpi_{\text{out}}$ , with  $\varpi_{\text{in}}$ ,  $\varpi_{\text{out}}$  the longitude of pericenters, and

$$\Phi_0 \equiv \frac{Gm_3 a^2}{a_{\text{out}}^3 (1 - e_{\text{out}}^2)^{3/2}}, \quad \varepsilon_{\text{oct}} \equiv \frac{m_1 - m_2}{m_{12}} \frac{a}{a_{\text{out}}} \frac{e_{\text{out}}}{1 - e_{\text{out}}^2}. \quad (35)$$

Various GR effects introduce extra apsidal precession

$$\left. \frac{de}{dt} \right|_{\text{extra}} = \dot{\omega}_{\text{extra}} \hat{\mathbf{L}} \times \mathbf{e}. \quad (36)$$

In terms of the effective potential,  $\dot{\omega}_{\text{extra}}$  is given by (see [49] and Appendix A)

$$\dot{\omega}_{\text{extra}} = -\frac{\sqrt{1 - e^2}}{e} \frac{1}{\mu\sqrt{Gm_{12}a}} \frac{\partial \Phi_{\text{extra}}}{\partial e}. \quad (37)$$

The effective  $\Phi_{\text{extra}}$  can be obtained from

$$\Phi_{\text{extra}} = - \int \dot{\omega}_{\text{extra}} \frac{e\mu\sqrt{Gm_{12}a}}{\sqrt{1 - e^2}} de. \quad (38)$$

Equation (37) is the canonical relations between Delaunay variables. Equations (36)-(38) can also apply to the outer binary. Consequently, the potential energy associated with the periastron advance in the inner and outer orbits are given by [49]

$$\Phi_{\text{GR,in}} = -\frac{3G^2 m_1 m_2 m_{12}}{c^2 a^2 \sqrt{1 - e^2}}, \quad (39)$$

$$\Phi_{\text{GR,out}} = -\frac{3G^2 m_{12} m_3 m_{123}}{c^2 a_{\text{out}}^2 \sqrt{1 - e_{\text{out}}^2}}. \quad (40)$$

Similarly, the potentials associated with the GR Effects I-III (Equations (12), (16) and (21)) due to the rotating SMBH are

$$\Phi_{\text{L}_{\text{out}}\text{S}_3} = \pm \frac{G^2 m_{12} (3m_{12} + 4m_3) S_3}{2c^2 n_{\text{out}} a_{\text{out}}^4 (1 - e_{\text{out}}^2)}, \quad (41)$$

$$\Phi_{\text{L}_{\text{in}}\text{L}_{\text{out}}} = \frac{G^3 m_1 m_2 m_3 (4m_{12} + 3m_3) \sqrt{1 - e^2}}{2c^2 n n_{\text{out}} a a_{\text{out}}^4 (1 - e_{\text{out}}^2)}, \quad (42)$$

$$\Phi_{\text{L}_{\text{in}}\text{S}_3} = \mp \frac{G^2 m_1 m_2 S_3 \sqrt{1 - e^2}}{c^2 n a a_{\text{out}}^3 (1 - e_{\text{out}}^2)^{3/2}}. \quad (43)$$

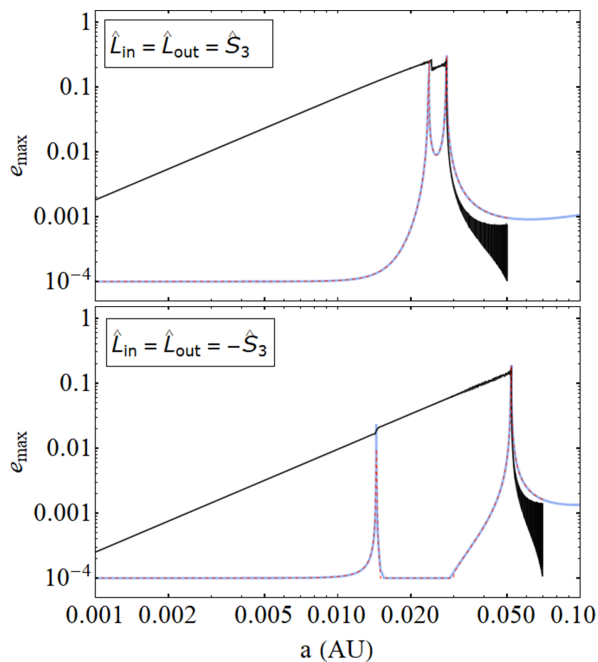


FIG. 2: The maximum eccentricity  $e_{\max}$  of the inner binary as a function of the semimajor axis  $a$  for systems starting with  $e_0 = 0$  and  $e_{\text{out},0} = 0.7$ . The system parameters are the same as in Figure 1. The black and blue lines are the results from numerical integration with and without the GW emission. The red dashed lines are achieved by the analytical formula according to the conservation laws.

In Equations (41) and (43), the upper (lower) sign refers to the  $\hat{S}_3 = \hat{L}$  ( $\hat{S}_3 = -\hat{L}$ ) case. The detailed derivation of the potentials is presented in Appendix A.

In the absence of dissipation (no GW), the total energy  $\Phi_{\text{tot}}$  (the sum of Equation (34) and (39)-(43)) is conserved. This energy conservation, together with angular momentum conservation,  $L_{\text{tot}} = L + L_{\text{out}} = \text{constant}$ , completely determine the secular evolution of the triple system.

Suppose  $e = 0$  and  $e_{\text{out}} = e_{\text{out},0}$  at  $t = 0$ , we can use the conservation of  $L_{\text{tot}}$  and  $\Phi_{\text{tot}}$  to determine  $e_{\max}$ , the maximum eccentricity attained by the inner binary. Note that since  $L_{\text{out}} \gg L$ , conservation of  $L_{\text{tot}}$  implies

$$e_{\text{out}} \simeq e_{\text{out},0} + \frac{1 - e_{\text{out},0}^2}{e_{\text{out},0}} \frac{L - L_0}{L_{\text{out},0}}, \quad (44)$$

where  $L_0$  and  $L_{\text{out},0}$  are the initial values of  $L$  and  $L_{\text{out}}$ , respectively. Solving the energy and angular momentum conservation laws (Equation (44)) yields  $e$  as a function of  $\Delta\varpi$ . The maximum eccentricity  $e_{\max}$  is achieved at either  $\Delta\varpi = 0$  or  $\pi$ , depending on the initial value of  $\Delta\varpi$ , and whether  $\Delta\varpi$  librates or circulates.

Figure 2 shows  $e_{\max}$  obtained by different methods as a function of  $a$  where the parameters are the same as in Figure 1. Here, the black solid lines are from the numerical integrations including the GW emission, while the

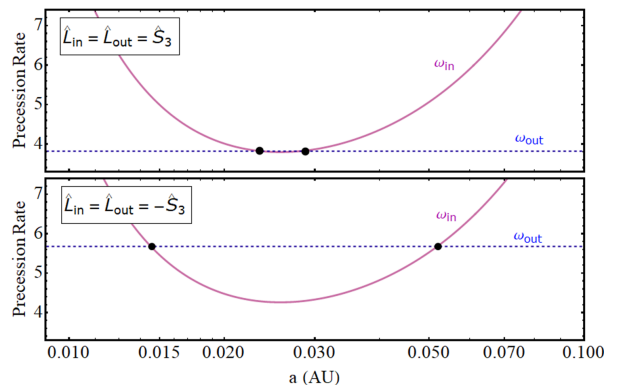


FIG. 3: The apsidal precession rates of the inner and outer binaries (Equations 45 and 46) as a function of  $a$ . The system parameters are the same as Figure 1. The black dots represent the resonance location where  $\omega_{\text{in}} = \omega_{\text{out}}$ .

the blue solid lines are achieved by integrating the equations without the GW radiation. We evolve the system for about  $\sim 10^3$  yrs for a given semimajor axis  $a$  and record  $e_{\max}$  during the evolution. The red dashed lines are the analytical prediction using the two conservation laws.

The numerical result (without the GW) are in a good agreement with the analytical calculation. We see that there are two evident peaks of  $e_{\max}$  in the blue and red dashed lines, indicating the resonance arises twice (see also Figure 3). However, in the “real” evolution of the system (i.e. with GW), the eccentricity preserves the memory of the excitation: Once the growth in  $e$  happens, the orbit can only be circularized by GW emission gradually.

### C. Eccentricity Excitation in coplanar System

Our analysis in Section IV A for linear (low- $e$ ) systems shows that the inner binary attains a peak eccentricity at the resonance  $\omega_{\text{in}} = \omega_{\text{out}}$ . For finite eccentricities, the resonance is not precise, but we expect a similar peak eccentricity occurs when  $\omega_{\text{in}} = \omega_{\text{out}}$ , with

$$\omega_{\text{in}} = \omega_{\text{LK},\text{in}} + \omega_{\text{GR},\text{in}} + \omega_{L_{\text{in}}L_{\text{out}}}^{(\text{GR})} \mp 2\omega_{L_{\text{in}}S_3}, \quad (45)$$

$$\omega_{\text{out}} = \omega_{\text{GR},\text{out}} \mp 2\omega_{L_{\text{out}}S_3} - 2\omega_{L_{\text{out}}L_{\text{in}}}^{(\text{GR})} \pm 6\omega_{S_3L_{\text{in}}}, \quad (46)$$

where the various frequencies include the dependence of finite  $e_{\text{out}} \simeq e_{\text{out},0}$ . Note that in Equation (46), the last two terms are much smaller than the corresponding terms in Equation (45) since  $L_{\text{in}}/L_{\text{out}} \ll 1$ .

Figure 3 shows  $\omega_{\text{in}}$  and  $\omega_{\text{out}}$  as a function of  $a$  for the examples depicted in Figure 1. When  $a$  is relatively large, the Newtonian interaction is strong and  $\omega_{\text{LK},\text{in}}$  is the dominated source in  $\omega_{\text{in}}$ . So we have  $\omega_{\text{in}} \gg \omega_{\text{out}}$ . On the other hand, near the merger of the inner binary ( $a$  is small), the GR effect becomes important and dominate the precession, leading to  $\omega_{\text{in}} \ll \omega_{\text{out}}$ . In between,

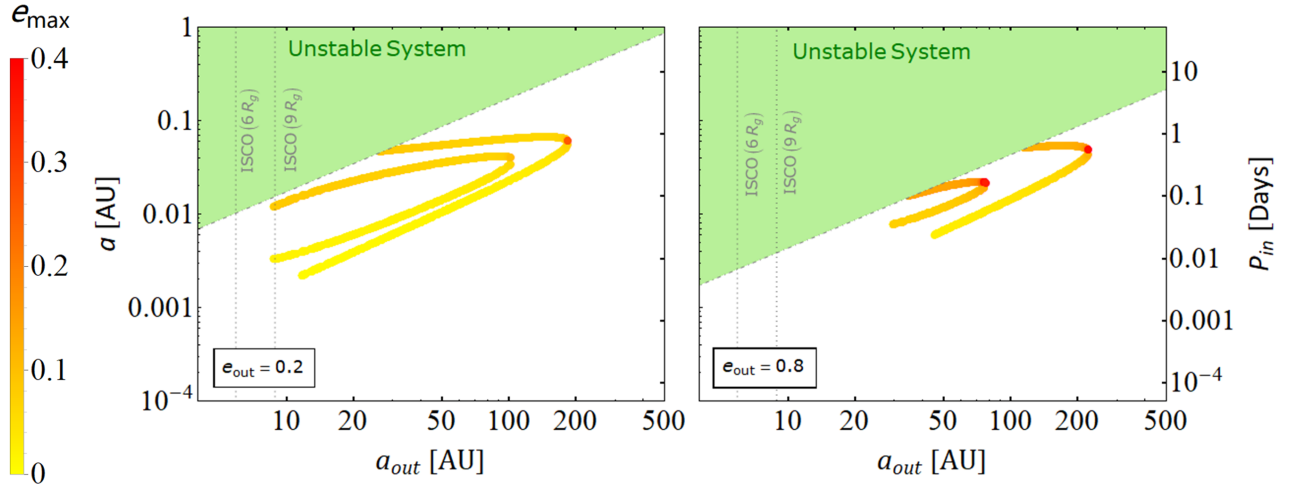


FIG. 4: Parameter space in the  $a - a_{\text{out}}$  plane, as well as the orbital period of the inner binary  $P_{\text{in}} - a_{\text{out}}$  plane, where the apsidal precession resonance occurs. The parameters are  $m_1 = 30M_\odot$ ,  $m_2 = 20M_\odot$ , and  $m_3 = 10^8 M_\odot$ . The outer binary is set up with two different eccentricities,  $e_{\text{out}} = 0.2$  for the left panel and  $e_{\text{out}} = 0.8$  for the right panel. The green region corresponds to the dynamically unstable triple systems. The dotted line indicates the innermost stable circular orbits (ISCO) for the outer binary, where  $R_g = (Gm_3)/c^2$ . The color-coded dots represent the values of the maximum eccentricity of the inner binary (with negligible initial eccentricity) due to the resonance, as calculated by energy and angular momentum conservations. Here, the inner and outer curves are from the triple systems with aligned and anti-aligned  $\hat{\mathbf{S}}_3$ , respectively.

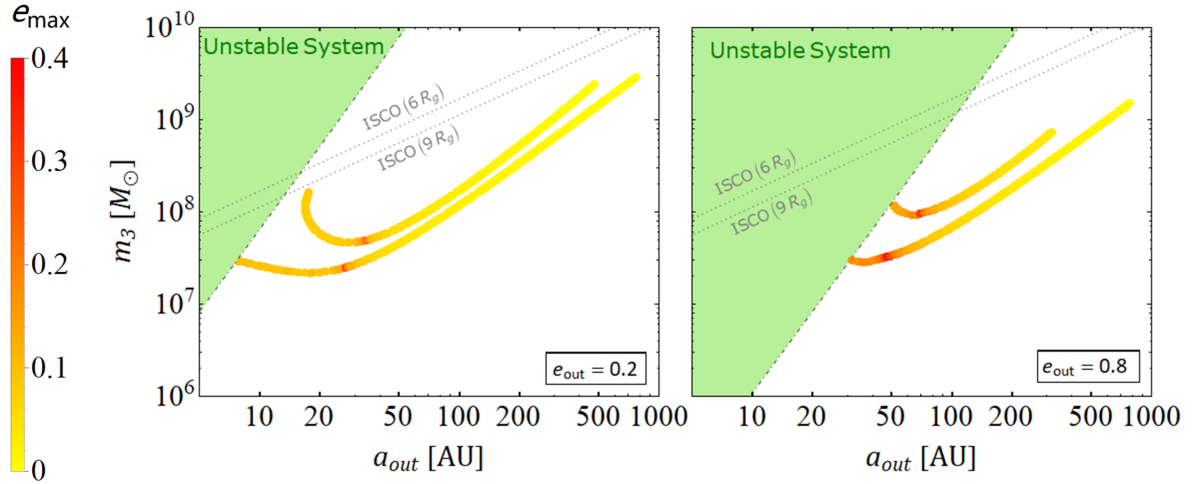


FIG. 5: Same as Figure 4, but in the  $m_3 - a_{\text{out}}$  plane, for  $a = 0.02$  AU.

we see that  $\omega_{\text{in}}$  crosses  $\omega_{\text{out}}$  twice, creating two ‘‘apsidal precession resonances’’ during the orbital decay.

#### D. Parameter Space

For a given set of system parameters, the criterion of apsidal precession resonance ( $\omega_{\text{in}} = \omega_{\text{out}}$ ) provides a good estimation on the resonance radius (resonance occurs at the location  $a = a_{\text{in,Res}}$  for a given  $a_{\text{out}}$ ; or  $a_{\text{out}} = a_{\text{out,Res}}$  for a given  $a$ ). Combining the analytical analysis in Section IV B, we can predict the maximum eccentricity of the inner binary at resonance.

Figure 4 illustrates the level of eccentricity excitation

in the  $a(P_{\text{in}}) - a_{\text{out}}$  plane for the given  $m_3$  and  $e_{\text{out}}$ . The green region corresponds to the space where the triple system is dynamically unstable, where the dot-dashed line is the instability limit according to [70]. The dotted lines indicate the innermost stable circular orbits (ISCO) for the outer binary, where  $R_g = (Gm_3)/c^2$  (the ISCO ranges from  $R_g$  to  $9R_g$  depending on the spin magnitude and orientation relative to the orbit). The color-coded dots denote the locations ( $a_{\text{in,Res}}$ ) at resonance and the values of  $e_{\text{max}}$ . The inner part apply to the systems with  $\hat{\mathbf{L}} = \hat{\mathbf{L}}_{\text{out}} = \hat{\mathbf{S}}_3$  and outer part  $\hat{\mathbf{L}} = \hat{\mathbf{L}}_{\text{out}} = -\hat{\mathbf{S}}_3$ .

We see that in the left panel of Figure 4, for the resonance to occur, the BHB must be close to the SMBH. In the case of aligned  $\hat{\mathbf{S}}_3$ , two locations of  $a_{\text{in,Res}}$  tend to con-

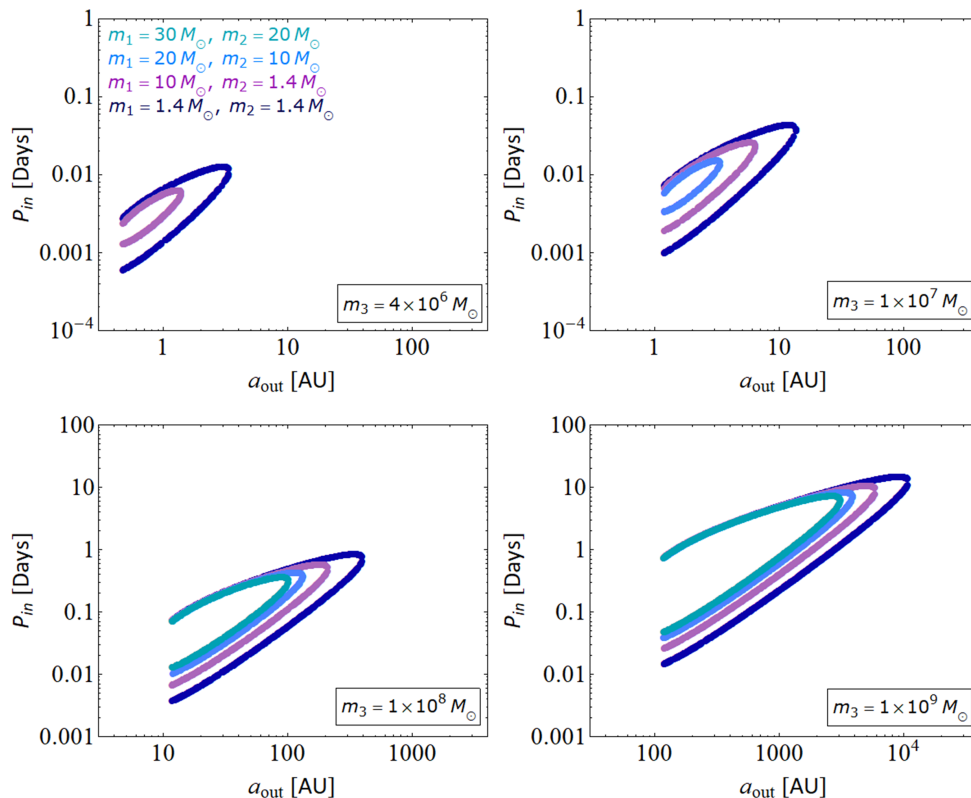


FIG. 6: Similar to Figure 4, but for the coplanar triple systems with aligned  $\hat{\mathbf{S}}_3$ . Here, we only show the systems satisfying the stability criterion and outside the ISCO. The outer eccentricity  $e_{\text{out}}$  is set to be 0.5 in all cases. We select different BH binary masses and SMBH mass, as labeled.

verge as  $a_{\text{out}}$  increases. The maximum  $e_{\text{max}}$  is achieved at the largest  $a_{\text{out}}$ . Furthermore, the eccentricity of the outer binary is crucial to produce significant  $e_{\text{max}}$  (as shown in the right panel).

Figure 5 shows the similar results but in the  $m_3 - a_{\text{out}}$  plane (with  $a$  fixed at 0.02 AU). The upper and lower color-coded dots are from the case of aligned and anti-aligned  $\hat{\mathbf{S}}_3$ , respectively. We find that the apsidal precession resonance is expected for a wide range of  $m_3$ . In particular, small  $m_3$  leads to larger values of  $e_{\text{max}}$  for a given  $a$  and  $e_{\text{out}}$ .

Figure 6 displays the resonance locations for four types of inner binaries (as labeled) in  $P_{\text{in}} - a_{\text{out}}$  plane, with four different SMBH masses. Note that we only restrict to the configuration where  $\hat{\mathbf{S}}_3$  is aligned with  $\hat{\mathbf{L}}_{\text{out}}$ , and have considered the criteria of stability [70] and ISCO. We see that, in terms of the occurrence of resonances, the small mass SMBH (top left panel) favors the low mass binary, especially the BH-NS binary and NS-NS binary. To produce resonance, these binaries must be concentrated in the inner-most region ( $\sim$ AU) around the SMBH. Since the BHB emits GW in the low frequency range before chirping to the LIGO band, if the time evolution on the binary eccentricity could be measured (e.g. sources near the Galactic center), it would provide a useful test for the binary formation channels. As the mass of the SMBH in-

creases, the apsidal precession resonance can emerge for the high mass binaries, and the regions of interest are located farther from the SMBH, as shown in other panels of Figure 6.

## V. RESONANCE IN THE INCLINED SYSTEMS

In this section, we extend our exploration to the general cases of mutually inclined inner/outer binaries, and misaligned spin of SMBH with respect to  $\hat{\mathbf{L}}_{\text{out}}$ . Since no simple analytical result can be derived, we sample  $a$  to determine the resonance location numerically for given outer binary parameters.

We first consider the same example as in Figure 1 (with aligned  $\hat{\mathbf{S}}_3$ ), but increase the initial inclination to the higher values. We integrate the secular equations of motion with no GW radiation, evolving the system for  $\sim 10^3$  yrs, and record  $e_{\text{max}}$  during the evolution. The results are shown in the upper panel of Figure 7. Compared to the fiducial example (black lines; the same as in Figure 2), we see that the resonance locations change and spread for larger inclinations. As  $I_0$  approaches  $40^\circ$ , the dynamics is largely determined by the LK oscillations when  $a \gtrsim 0.05$  AU (For smaller  $a$ 's, LK oscillations are suppressed), and



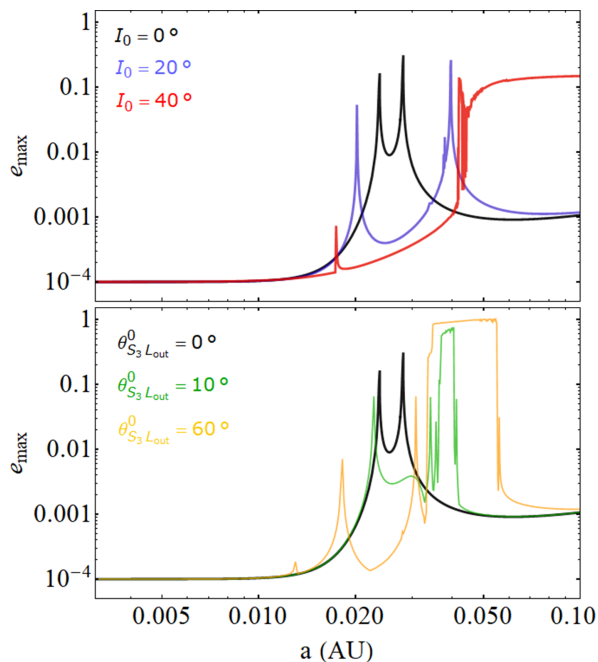


FIG. 7: The maximum eccentricity  $e_{\max}$  as a function of the inner binary semimajor axis  $a$ , obtained by integrating the octupole equations of motion and including the GR effects (but no GW emission). The upper panel shows the results from various initial inclinations (as labeled) and aligned  $\hat{\mathbf{S}}_3$  (parallel to  $\hat{\mathbf{L}}_{\text{out}}$ ). The lower panel shows the results from different initial  $\hat{\mathbf{S}}_3 - \hat{\mathbf{L}}_{\text{out}}$  misalignment angles (as labeled) and coplanar tripla. The other parameters are the same as in Figure 1.

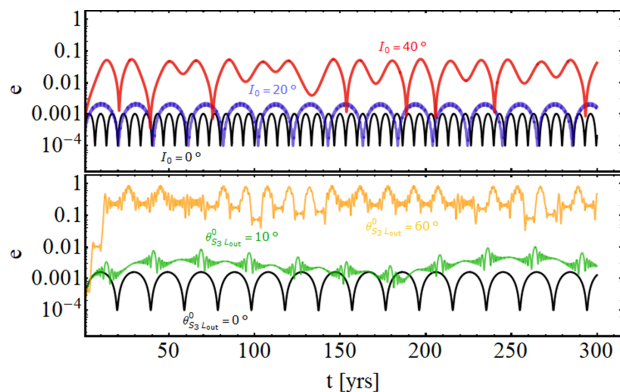


FIG. 8: Evolution examples of the orbital eccentricity in the inner binary. The parameters are picked from the cases in Figure 7, and  $a = 0.046\text{AU}$  (upper panel) and  $a = 0.0363\text{AU}$  (lower panel).

the eccentricity excitation due to resonance tends to be erased.

We can see several examples of the eccentricity evolution in the upper panel of Figure 8, where  $a$  is fixed to be  $0.046\text{ AU}$ . The maximum eccentricity varies. The irregular behavior in the case of  $I_0 = 40^\circ$  arises due to

the combined influences of Effects I-III.

Alternatively, we vary the spin orientation of the SMBH, choosing the initial misalignment angle between  $\hat{\mathbf{S}}_3$  and  $\hat{\mathbf{L}}_{\text{out}}$  (i.e.,  $\theta_{\hat{\mathbf{S}}_3 \hat{\mathbf{L}}_{\text{out}}}^0$ ) to be  $0^\circ$ ,  $10^\circ$  and  $60^\circ$ , while keeping the mutual binary inclination angle to zero. The results are shown in the lower panel of Figure 7. Somewhat surprisingly, in this case,  $e_{\max}$  is sensitive to  $\theta_{\hat{\mathbf{S}}_3 \hat{\mathbf{L}}_{\text{out}}}^0$  and it can grow to larger values, approaching the unity. This is because Effect I plays a crucial role, and LK oscillations can be triggered (especially for  $\theta_{\hat{\mathbf{S}}_3 \hat{\mathbf{L}}_{\text{out}}}^0 = 60^\circ$ ) due to an inclination resonance [e.g., 61]. To illustrate the  $e$  evolution, in the lower panel of Figure 8, we see the growth of  $e$  becomes chaotic for the fixed  $a = 0.0363\text{ AU}$ .

We now include the dissipative effect of gravitational radiation. If we adopt the slightly inclined outer binary and aligned (or anti-aligned)  $\hat{\mathbf{S}}_3$ , the system can still encounter the apsidal precession resonance. Figure 9 shows an example of a merging BHB with the inclined SMBH ( $I_0 = 10^\circ$ ). The initial misalignment angles between  $\hat{\mathbf{L}}_{\text{out}}$  and  $\hat{\mathbf{S}}_3$  are  $10^\circ$  (left panel) and  $170^\circ$  (right panel), respectively. We find that the behaviors of  $e$  and  $e_{\text{out}}$ , in particular the excitation of the inner binary eccentricity, are more significant than the case of coplanar triple. When the resonance is encountered during the orbital decay,  $e$  increases while  $e_{\text{out}}$  decreases. The systems have the maximum eccentricities in excess of 0.81.

If the triple systems are initialized with arbitrary  $I_0$  and  $\theta_{\hat{\mathbf{S}}_3 \hat{\mathbf{L}}_{\text{out}}}^0$ , the evolution may become chaotic, and the eccentricity of the inner binary can easily grow to close to unity [e.g., 61]. Such ‘‘GR-enhanced’’ channel may play an important role in BHB mergers. A comprehensive parameter space study is beyond the scope of this paper and we leave it to a future work.

## VI. DISCUSSION AND CONCLUSION

In this paper, we have studied the dynamics of compact BH-BH binaries under the influence of a nearby rotating SMBH in a hierarchical triple configuration. We have presented the general secular equations of motion that govern the evolution of the (BH-BH)-SMBH triple system, including various general relativistic (GR) effects that couple the inner and outer orbits and the spin of the SMBH (Section II). These post-Newtonian equations of motion are derived and extended from previous work on binaries with spinning bodies [65]. In our recent work [61], we have shown that several of these GR effects can significantly influence the rate of tertiary induced binary mergers via Lidov-Kozai mechanism. In this paper, we focus on systems with small mutual inclinations such that Lidov-Kozai oscillation does not happen. We show that compact binaries near a SMBH can experience an ‘‘apsidal precession resonance’’, where the pericenter precession rate of the inner binary matches that of the outer binary. Both precessions are driven by the combined effects of Newtonian gravitational interaction and general relativity. The resonance results in an efficient ‘‘transfer’’

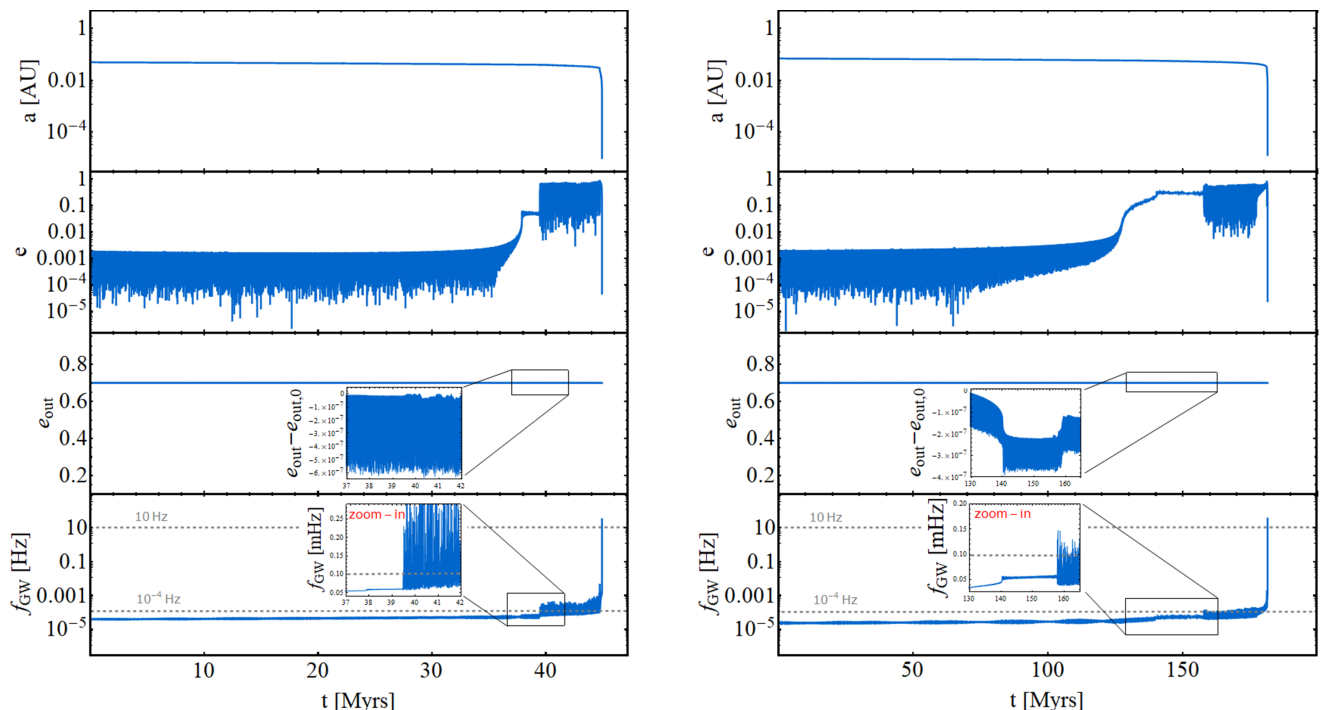


FIG. 9: Similar to Figure 1, but for triple systems with finite initial binary inclinations and  $\hat{\mathbf{S}}_3 - \hat{\mathbf{L}}_{\text{out}}$  misalignment angles:  $I_0 = 10^\circ$ ,  $\theta_{\text{S}_3\text{L}_{\text{out}}}^0 = 10^\circ$  (left) and  $\theta_{\text{S}_3\text{L}_{\text{out}}}^0 = 170^\circ$  (right). The other parameters are the same as in Figure 1. The qualitative behavior of the inclined systems is similar to the coplanar systems, but the maximum eccentricities due to resonance are larger.

of eccentricity from the outer binary to the inner binary, leading to eccentricity growth of the inner binary. An example of the eccentricity growth due to apsidal precession resonance during binary merger near a SMBH is shown in in Figure 1.

We provide analytical analysis for coplanar systems with small eccentricities (linear theory; Section IV A) and finite eccentricities (non-linear theory; Section IV B). The linear theory gives a useful criterion for the resonance (Equations (32), (45) and (46)), but the non-linear theory is needed to accurately predict the value of maximum eccentricity excitation (see Figure 2). The growth of the eccentricity in the inner binary at resonance can be understood as “angular momentum exchange” (i.e., eccentricity exchange) between the inner and outer binaries. For the systems studied in this paper ( $m_{\text{SMBH}} = m_3 \gg m_1, m_2$ ), even a weakly eccentric outer orbit (SMBH’s orbit) can excite appreciable eccentricity in the inner BH-BH binary, and the peak eccentricity increases as the outer binary becomes more eccentric (see Figure 4).

The eccentricity growth due to apsidal resonance generally operates for triple systems with small mutual inclinations (in contrast to Lidov-Kozai oscillations, which require high mutual inclinations) and allows for generally misaligned spin orientations of the SMBH. (see Figure 7 and 8). The GR effects (especially Effect I; see Equations (11)-(14)) play an important role, and can make the orbital evolution of the BH binary chaotic. The ec-

entricity of the merging binary can attain a larger value compared to the corresponding coplanar case (see Figure 9).

The apsidal precession resonance can occur while the binary is emitting gravitational waves in the low-frequency band, thus potentially detectable by future gravitational wave detectors operating at low frequencies, such as LISA, DECIGO [71] and TianQin [72]. Binary mergers near the Galactic Center would be of great interest, particularly if the eccentricity evolution can be tracked. Of course, whether stellar BBHs actually exist so close to the SMBH is unknown. Such close-in BBHs may result from mass segregation and the scatterings. A SMBH could also tidally capture a BHB to a bound orbit, and the BHB would inspiral towards the SMBH in a close orbit due to gravitational radiation. A complete study of this topic is beyond the scope of this paper. On the other hand, the apsidal precession resonance may play a role in the scenario of BH binary merger in the Active Galactic Nuclei disk [e.g., 16]. In this case, a BH binary aligns its orbit with the disk, and moves to the migration trap close to the central SMBH. The final configuration of (BH-BH)-SMBH system may then satisfy the criterion of resonance studied in this paper.

## VII. ACKNOWLEDGMENTS

This work is supported in part by the NSF grant AST-1715246 and NASA grant NNX14AP31G.

- 
- [1] B. P. Abbott, R. Abbott, T. D. Abbott, F. Acernese, K. Ackley, C. Adams, T. Adams, P. Addesso, R. X. Adhikari, V. B. Adya, et al., *Phys. Rev. X* **9**, 031040 (2019).
- [2] B. P. Abbott, R. Abbott, T. D. Abbott, F. Acernese, K. Ackley, C. Adams, T. Adams, P. Addesso, R. X. Adhikari, V. B. Adya, et al., arXiv:1811.12940.
- [3] B. Zackay, T. Venumadhav, L. Dai, J. Roulet, and M. Zaldarriaga, *Phys. Rev. D* **100**, 023007 (2019).
- [4] T. Venumadhav, B. Zackay, J. Roulet, L. Dai, and M. Zaldarriaga, arXiv:1904.07214.
- [5] B. Zackay, L. Dai, T. Venumadhav, J. Roulet, and M. Zaldarriaga, arXiv:1910.09528.
- [6] V. M. Lipunov, K. A. Postnov, and M. E. Prokhorov, *Astron. Lett.* **23**, 492 (2019).
- [7] V. M. Lipunov, V. Kornilov, E. Gorbovskoy, D. A. H. Buckley, N. Tiurina, P. Balanutsa, A. Kuznetsov, J. Greiner, V. Vladimirov, D. Vlasenko et al., *Mon. Not. R. Astron. Soc.* **465**, 3656 (2017).
- [8] P. Podsiadlowski, S. Rappaport, and Z. Han, *Mon. Not. R. Astron. Soc.* **341**, 385 (2003).
- [9] K. Belczynski, M. Dominik, T. Bulik, R. O’Shaughnessy, C. Fryer, and D. E. Holz, *Astrophys. J. Lett.* **715**, L138 (2010).
- [10] K. Belczynski, D. E. Holz, T. Bulik, and R. O’Shaughnessy, *Nature (London)* **534**, 512 (2016).
- [11] M. Dominik, K. Belczynski, C. Fryer, D. E. Holz, E. Berti, T. Bulik, I. Mandel, and R. O’Shaughnessy, *Astrophys. J.* **759**, 52 (2012).
- [12] M. Dominik, K. Belczynski, C. Fryer, D. E. Holz, E. Berti, T. Bulik, I. Mandel, and R. O’Shaughnessy, *Astrophys. J.* **779**, 72 (2013).
- [13] M. Dominik, E. Berti, R. O’Shaughnessy, I. Mandel, K. Belczynski, C. Fryer, D. E. Holz, T. Bulik, and F. Panarale, *Astrophys. J.* **806**, 263 (2015).
- [14] I. Mandel and S. E. De Mink, *Mon. Not. R. Astron. Soc.* **458**, 2634 (2016).
- [15] P. Marchant, N. Langer, P. Podsiadlowski, T. M. Tauris, and T. J. Moriya, *Astron. Astrophys.* **588**, A50 (2016).
- [16] I. Bartos, B. Kocsis, Z. Haiman, and S. Mrka, *Astrophys. J.* **835**, 165 (2017).
- [17] S. F. P. Zwart and S. L. W. McMillan, *Astrophys. J. Lett.* **528**, L17 (2000).
- [18] R. M. O’Leary, F. A. Rasio, J. M. Fregeau, N. Ivanova, and R. O’Shaughnessy, *Astrophys. J.* **637**, 937 (2006).
- [19] M. C. Miller and V. Lauburg, *Astrophys. J.* **692**, 917 (2009).
- [20] S. Banerjee, H. Baumgardt, and P. Kroupa, *Mon. Not. R. Astron. Soc.* **402**, 371 (2010).
- [21] J. M. B. Downing, M. J. Benacquista, M. Giersz, and R. Spurzem, *Mon. Not. R. Astron. Soc.* **407**, 1946 (2010).
- [22] B. M. Ziosi, M. Mapelli, M. Branchesi, and G. Tormen, *Mon. Not. R. Astron. Soc.* **441**, 3703 (2014).
- [23] C. L. Rodriguez, M. Morscher, B. Pattabiraman, S. Chatterjee, C.-J. Haster, and F. A. Rasio, *Phys. Rev. Lett.* **115**, 051101 (2015).
- [24] J. Samsing and E. Ramirez-Ruiz, *Astrophys. J. Lett.* **840**, L14 (2017).
- [25] J. Samsing and D. J. D’Orazio, *Mon. Not. R. Astron. Soc.* **481**, 5445 (2018).
- [26] C. L. Rodriguez, P. Amaro-Seoane, S. Chatterjee, and F. A. Rasio, *Phys. Rev. Lett.* **120**, 151101 (2018).
- [27] L. Gondán, B. Kocsis, P. Raffai, and Z. Frei, *Astrophys. J.* **860**, 5 (2018).
- [28] O. Blaes, M. H. Lee, and A. Socrates, *Astrophys. J.* **578**, 775 (2002).
- [29] M. C. Miller and D. P. Hamilton, *Astrophys. J.* **576**, 894 (2002).
- [30] L. Wen, *Astrophys. J.* **598**, 419 (2003).
- [31] F. Antonini and H. B. Perets, *Astrophys. J.* **757**, 27 (2012).
- [32] F. Antonini, S. Toonen, and A. S. Hamers, *Astrophys. J.* **841**, 77 (2017).
- [33] K. Silsbee and S. Tremaine, *Astrophys. J.* **836**, 39 (2017).
- [34] B. Liu, and D. Lai, *Astrophys. J. Lett.* **846**, L11 (2017).
- [35] B. Liu, and D. Lai, *Astrophys. J.* **863**, 68 (2018).
- [36] L. Randall and Z.-Z. Xianyu, *Astrophys. J.* **853**, 93 (2018).
- [37] B.-M. Hoang, S. Naoz, B. Kocsis, F. A. Rasio, and F. Dosopoulou, *Astrophys. J.* **856**, 140 (2018).
- [38] B. Liu, D. Lai, and Y.-H. Wang, *Astrophys. J.* **881**, 41 (2019).
- [39] M. L. Lidov, *Planetary and Space Science* **9**, 719 (1962).
- [40] Y. Kozai, *Astron. J.* **67**, 591 (1962).
- [41] S. Naoz, *Annu. Rev. Astron. Astrophys.* **54**, 441 (2016).
- [42] X. Fang, T. A. Thompson, and C. M. Hirata, *Mon. Not. R. Astron. Soc.* **476**, 4234 (2018).
- [43] B. Liu and D. Lai, *Mon. Not. R. Astron. Soc.* **483**, 4060 (2019).
- [44] G. Fragione and B. Kocsis, *Mon. Not. R. Astron. Soc.* **486**, 4781 (2019).
- [45] M. Zevin, J. Samsing, C. Rodriguez, C.-J. Haster, and E. Ramirez-Ruiz, *Astrophys. J.* **871**, 91 (2019).
- [46] A. S. Hamers and D. Lai, *Mon. Not. Roy. Astron. Soc.* **470**, 1657 (2017).
- [47] C. Petrovich and F. Antonini, *Astrophys. J.* **846**, 146 (2017).
- [48] G. Fragione, E. Grishin, N. W. C. Leigh, H. B. Perets, and R. Perna, *Mon. Not. R. Astron. Soc.* **488**, 47 (2019).
- [49] D. Fabrycky and S. Tremaine, *Astrophys. J.* **669**, 1298 (2007).
- [50] B. Liu, D. J. Muñoz, and D. Lai, *Mon. Not. Roy. Astron. Soc.* **447**, 747 (2015).
- [51] K. R. Anderson, D. Lai, and N. I. Storch, *Mon. Not. Roy. Astron. Soc.* **467**, 3066 (2017).
- [52] E. B. Ford, B. Kozinsky, and F. A. Rasio, *Astrophys. J.* **535**, 385 (2000).
- [53] R. A. Mardling, *Mon. Not. R. Astron. Soc.* **382**, 1768 (2007).
- [54] S. Naoz, B. Kocsis, A. Loeb, and N. Yunes, *Astrophys. J.* **773**, 187 (2013).

- [55] C. M. Will, Phys. Rev. D **89**, 044043 (2014).  
 [56] C. M. Will, Phys. Rev. Lett. **120**, 191101 (2018).  
 [57] H. Lim, and C. L. Rodriguez, arXiv:2001.03654.  
 [58] B. Liu, D. Lai, and Y.-F. Yuan, Phys. Rev. D **92**, 124048 (2015).  
 [59] R. M. O’Leary, B. Kocsis, and A. Loeb, Mon. Not. Roy. Astron. Soc. **395**, 2127 (2009).  
 [60] N. W. C. Leigh, A. M. Geller, B. McKernan, K. E. S. Ford, M.-M. Mac Low, J. Bellovary, Z. Haiman, W. Lyra, J. Samsing, M. O’Dowd, B. Kocsis, and S. Endlich, Mon. Not. R. Astron. Soc. **474**, 5672 (2018).  
 [61] B. Liu, D. Lai, and Y.-H. Wang, Astrophys. J. Lett. **883**, L7 (2019).  
 [62] J. H. VanLandingham, M. C. Miller, D. P. Hamilton, and D. C. Richardson, Astrophys. J. **828**, 77 (2016).  
 [63] A. S. Hamers, B. Bar-Or, C. Petrovich, and F. Antonini, Astrophys. J. **865**, 2 (2018).  
 [64] P. C. Peters, Phys. Rev. **136**, B1224 (1964).  
 [65] B. M. Barker and R. F. O’Connell, Phys. Rev. D **12**, 329 (1975).  
 [66] É. Racine, Phys. Rev. D **78**, 044021 (2008).  
 [67] Y. Fang and Q. G. Huang, Phys. Rev. D **99**, 103005 (2019).  
 [68] C. D. Murray, and S. F. Dermott, Solar System Dynamics, Cambridge U. Press, NY (1999).  
 [69] S. Naoz, W. M. Farr, Y. Lithwick, and F. A. Rasio, Mon. Not. R. Astron. Soc. **431**, 2155 (2013).  
 [70] L. G. Kiseleva, S. J. Aarseth, P. P. Eggleton, and R. de La Fuente Marcos, in ASP Conf. Ser. 90, The Origins, Evolution, and Destinies of Binary Stars in Clusters, ed. E. F. Milone and J.-C. Mermilliod (San Francisco, CA: ASP), 433 (1996).  
 [71] S. Kawamura et al., Class. Quant. Grav. **28**, 094011 (2011).  
 [72] J. Luo et al. (TianQin Collaboration), Class. Quant. Grav. **33**, 035010 (2016).

## Appendix A: The Effective Potentials of GR Effects

In the hierarchical coplanar triple system, the secular Hamiltonian is given by

$$\begin{aligned} \mathcal{H} &= \mathcal{H}_1 + \mathcal{H}_2 + \Phi \\ &= -\frac{Gm_1m_2}{2a} - \frac{Gm_{12}m_3}{2a_{\text{out}}} + \Phi_N + \Phi_{\text{extra}}, \end{aligned} \quad (\text{A1})$$

where  $\Phi_N$  is given by Equation (34), and  $\Phi_{\text{extra}}$  is the effective potential due to various GR effects. For the coplanar systems ( $\hat{\mathbf{L}} = \hat{\mathbf{L}}_{\text{out}}$ ), we have  $\mathcal{H} = \mathcal{H}(\varpi_{\text{in}}, L_{\text{in}}, \varpi_{\text{out}}, L_{\text{out}})$ , where  $\varpi_{\text{in}}$  and  $\varpi_{\text{out}}$  are the longitude of pericenter of the inner and outer binaries, respectively, and  $L_{\text{in}} = \mu\sqrt{Gm_{12}a(1-e^2)}$ ,  $L_{\text{out}} = \mu_{\text{out}}\sqrt{Gm_{123}a_{\text{out}}(1-e_{\text{out}}^2)}$  are the respective canonical momenta. The canonical equations of motion for the inner and outer orbits are

$$\dot{\varpi}_{\text{in}} = \frac{\partial \mathcal{H}}{\partial L_{\text{in}}}, \quad \dot{L}_{\text{in}} = -\frac{\partial \mathcal{H}}{\partial \varpi_{\text{in}}}, \quad (\text{A2})$$

$$\dot{\varpi}_{\text{out}} = \frac{\partial \mathcal{H}}{\partial L_{\text{out}}}, \quad \dot{L}_{\text{out}} = -\frac{\partial \mathcal{H}}{\partial \varpi_{\text{out}}}. \quad (\text{A3})$$

Since  $\mathcal{H}$  depends on  $\varpi_{\text{in}}$  and  $\varpi_{\text{out}}$  through  $(\varpi_{\text{in}} - \varpi_{\text{out}})$  (see Equation (34)), the second equations in (A2) and

(A3) yield angular momentum conservation

$$L_{\text{in}} + L_{\text{out}} = \text{constant}. \quad (\text{A4})$$

In vector form, the first equations in (A2) and (A3) imply that the apsidal precession due to  $\Phi_{\text{extra}}$  is given by

$$\left. \frac{d\mathbf{e}}{dt} \right|_{\text{extra}} = \dot{\varpi}_{\text{extra}}^{(\text{in})} \hat{\mathbf{L}} \times \mathbf{e} \quad (\text{A5})$$

$$\left. \frac{d\mathbf{e}_{\text{out}}}{dt} \right|_{\text{extra}} = \dot{\varpi}_{\text{extra}}^{(\text{out})} \hat{\mathbf{L}}_{\text{out}} \times \mathbf{e}_{\text{out}}, \quad (\text{A6})$$

where

$$\dot{\varpi}_{\text{extra}}^{(\text{in})} = \frac{\partial \Phi_{\text{extra}}}{\partial L_{\text{in}}}, \quad \dot{\varpi}_{\text{extra}}^{(\text{out})} = \frac{\partial \Phi_{\text{extra}}}{\partial L_{\text{out}}}. \quad (\text{A7})$$

Thus, for a given apsidal precession rate, the ‘‘common’’ extra potential can be evaluated by

$$\Phi_{\text{extra}} = \int \dot{\varpi}_{\text{extra}}^{(\text{in})} dL_{\text{in}} = \int \dot{\varpi}_{\text{extra}}^{(\text{out})} dL_{\text{out}}. \quad (\text{A8})$$

Consider the various GR effects discussed in Section II. For Effect I, Equation (12) reduces to

$$\left. \frac{d\mathbf{e}_{\text{out}}}{dt} \right|_{L_{\text{out}}S_3} = (\mp 2\varpi_{L_{\text{out}}S_3}) \hat{\mathbf{L}}_{\text{out}} \times \mathbf{e}_{\text{out}}. \quad (\text{A9})$$

The upper (lower) sign refers to the  $\hat{\mathbf{S}}_3 = \hat{\mathbf{L}}$  ( $\hat{\mathbf{S}}_3 = -\hat{\mathbf{L}}$ ) case. Using (14), the effective potential can be obtained:

$$\begin{aligned} \Phi_{L_{\text{out}}S_3} &= \int (\mp 2\varpi_{L_{\text{out}}S_3}) \mu_{\text{out}} \sqrt{Gm_{123}a_{\text{out}}} d\sqrt{1-e_{\text{out}}^2} \\ &= \pm \frac{G^2 m_{12}(3m_{12} + 4m_3)S_3}{2c^2 n_{\text{out}} a_{\text{out}}^4 (1-e_{\text{out}}^2)}. \end{aligned} \quad (\text{A10})$$

For Effect II, Equations (16) and (18) reduce to

$$\left. \frac{d\mathbf{e}}{dt} \right|_{L_{\text{in}}L_{\text{out}}} = \varpi_{L_{\text{in}}L_{\text{out}}}^{(\text{GR})} \hat{\mathbf{L}}_{\text{out}} \times \mathbf{e}, \quad (\text{A11})$$

$$\left. \frac{d\mathbf{e}_{\text{out}}}{dt} \right|_{L_{\text{out}}L_{\text{in}}} = -2\varpi_{L_{\text{out}}L_{\text{in}}}^{(\text{GR})} \hat{\mathbf{L}}_{\text{out}} \times \mathbf{e}_{\text{out}}. \quad (\text{A12})$$

Using Equation (19), the common effective potential can be obtained:

$$\begin{aligned} \Phi_{L_{\text{in}}L_{\text{out}}} &= \int \varpi_{L_{\text{in}}L_{\text{out}}}^{(\text{GR})} \mu \sqrt{Gm_{12}a} d\sqrt{1-e^2} \\ &= \int (-2\varpi_{L_{\text{out}}L_{\text{in}}}^{(\text{GR})}) \mu_{\text{out}} \sqrt{Gm_{123}a_{\text{out}}} d\sqrt{1-e_{\text{out}}^2} \\ &= \frac{G^3 m_1 m_2 m_3 (4m_{12} + 3m_3) \sqrt{1-e^2}}{2c^2 n n_{\text{out}} a a_{\text{out}}^4 (1-e_{\text{out}}^2)}. \end{aligned} \quad (\text{A13})$$

For Effect III, Equations (21) and (23) reduce to

$$\left. \frac{d\mathbf{e}}{dt} \right|_{L_{\text{in}}S_3} = (\mp 2\varpi_{L_{\text{in}}S_3}) \hat{\mathbf{L}}_{\text{out}} \times \mathbf{e}, \quad (\text{A14})$$

$$\left. \frac{d\mathbf{e}_{\text{out}}}{dt} \right|_{S_3L_{\text{in}}} = (\pm 6\varpi_{S_3L_{\text{in}}}) \hat{\mathbf{L}}_{\text{out}} \times \mathbf{e}_{\text{out}}. \quad (\text{A15})$$

Again, the upper (lower) sign refers to the  $\hat{\mathbf{S}}_3 = \hat{\mathbf{L}}$  ( $\hat{\mathbf{S}}_3 = -\hat{\mathbf{L}}$ ) case. Using (24), the effective potential is given by

$$\begin{aligned}
\Phi_{L_{in}S_3} &= \int (\mp 2\varpi_{L_{in}S_3})\mu\sqrt{Gm_{12}a} d\sqrt{1-e^2} \\
&= \int (\pm 6\varpi_{S_3L_{in}})\mu_{out}\sqrt{Gm_{123}a_{out}} d\sqrt{1-e_{out}^2} \\
&= \mp \frac{G^2 m_1 m_2 S_3 \sqrt{1-e^2}}{c^2 n a a_{out}^3 (1-e_{out}^2)^{3/2}}. \tag{A16}
\end{aligned}$$